ELSEVIER

Journal of Power Sources 67 (1997) 69–84

JOURNAL OF POWER SOURCES

# Dynamic modelling of lead/acid batteries using impedance spectroscopy for parameter identification

P. Mauracher *, E. Karden

*Aachen University of Technology, Institute for Power Electronics and Electrical Drives, Jägerstraße 17–19, 52066 Aachen, Germany*

Received 28 August 1996; accepted 16 December 1996

**Abstract**

A precise battery model is set up that gives the terminal voltage as a function of current and time. The model structure is based on a Randles' equivalent circuit. The non-linear dependence of all equivalent-circuit elements on current and frequency is taken into account. Model parameters are determined by impedance spectroscopy with various superimposed direct currents. Detailed measurements show that this battery model calculates the terminal voltage of lead/acid batteries with a tolerance of less than ±0.2%. © 1997 Elsevier Science S.A.

*Keywords:* Battery modelling; Dynamic modelling; Concentration models; Lead/acid batteries

## 1. Introduction

The simulation of the energy consumption of electric vehicles requires precise battery models. Until now, phenomenological models of lead/acid batteries are usually applied. These models require many parameters. Despite this, the results of such models are rarely satisfying. Moreover, the high numerical expense caused by large parameter sets leads to an inefficient application of phenomenological models. Accordingly, this paper presents a battery model that is based on physical and chemical fundamentals. At first, the small-signal performance is evaluated (called 'differential performance'). After that, the large-signal characterization of the battery (called 'integral performance') is derived by integrating the equations that describe the differential performance. All calculations are numerically simple so that the model is well suited for simulation programs.

After setting the requirements for the battery model with respect to the practical use, the physical and chemical equations are built and applied to a lead/acid battery with an immobilized electrolyte. The resulting differential equations are solved in the frequency domain and their results are interpreted as electrotechnical quantities of an equivalent circuit. Then, the model parameters are derived for a Sonnenschein dry-fit traction block (Type 6V-160) with the help of the impedance spectroscopy. Finally, the battery model is verified by measurements on a traction battery under real driving conditions.

## 2. Requirements for the battery model

Since electric-vehicle driving usually does not take more than 2 h, the dynamic performance of the traction battery has to be regarded only down to frequencies of about 50 μHz. In order to calculate the energy consumption of vehicles, models are required with an accuracy that is better than ±0.5%. Therefore, the battery model has to represent the terminal voltage

* Corresponding author. E-mail: ka@isea.rwth-aachen.de


*PII* S0378-7753(97)02498-1

Table 1
Validity domain of the battery model

| | |
|---|---|
| Frequency | 10 Hz–10 μHz (discharging) 10 Hz–10 mHz (charging) |
| Voltage–amplitude tolerance | ±0.5% $V_N$ = ±10 mV/cell |
| Current | ±300 A |
| State-of-charge | 10%–90% |
| Not taken into account | Temperature, aging, variance in type and by production |

with a tolerance of less than ±10 mV per cell. At ±300 A, the maximum driving and braking current is approximately ten times the nominal 5 h current of the traction battery referred to in this paper.

The fact that all phenomena that influence battery performance depend on the state-of-charge (SOC) is only important for those batteries that are almost completely charged or nearly empty. In the case of about 10% up to 90% drawn charge, the influence of SOC may be ignored. In order to reduce the numerical expense, the SOC dependence of all overvoltages is neglected in this modelling.

Since the battery model is used for the simulation of vehicle driving only the discharging operation is modelled. The charging operation is only considered so far as it is necessary for intervening charging by regenerative braking. Therefore, the model is only valid for charging with frequencies higher than 10 mHz. Table 1 shows the validity domain of this battery model.

## 3. Structure of the battery model

The battery model is based on a Randles' equivalent circuit [1]. Given the case of no current flowing, the voltage adjusts to an equilibrium voltage $V_0$ that can be described as an ideal voltage source depending on the SOC. A constant equivalent resistance $R_i$ is used for modelling all conductive media of the battery.

The electrolytic double-layer capacitance is modelled by $C_D$. The Faraday branch of the equivalent circuit contains the charge-transfer resistance $R_D$ and two Warburg impedances $Z_{WI}$ and $Z_{WL}$ which model the diffusion within the electrolyte. The complete equivalent circuit of the lead/acid battery is shown in Fig. 1. Please note that nearly all circuit elements are non-linear.

Since all phenomena that influence battery performance exhibit a non-linear dependence on current, only a measurement of dynamic values is suitable. Impedance spectroscopy is well suited for such measurements unless the measuring instrument is able to supply the battery with direct currents of the order $I_4$ [2]. The classification of the results as different types of overvoltages can be easily achieved (Fig. 2 shows an example) [3].

The time constant that characterizes the performance of the charge-transfer reaction and double-layer capacitance is smaller by at least one order of magnitude than the time constants that occur in the concentration element (see Fig. 2). Therefore, the Randles' equivalent circuit is simplified as shown in Fig. 3 without changing the values of its elements.

In the following, each part of the battery model is described. Since the determination of $V_0$, $R_D$ and $C_D$ is based on fundamentals that could nearly all be taken from literature, the determination is only discussed briefly in this paper. By contrast, the diffusion modelled by Warburg impedances is described in detail, because of its strong dependence on frequency and current.

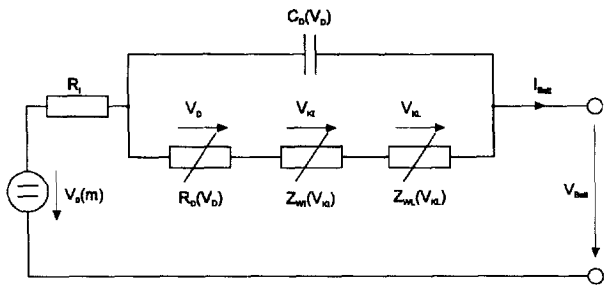


Fig. 1. Complete equivalent circuit of a lead/acid battery based on Randles' theory.

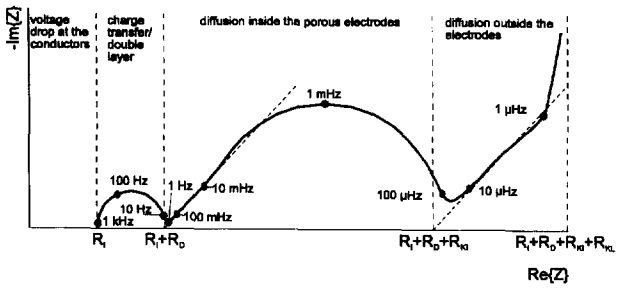


Fig. 2. Nyquist plot of lead/acid battery for small direct currents (idealized). The effects of various overvoltage mechanisms on the battery locus-diagram can be separated into different frequency bands.

### 3.1. Modelling the equilibrium voltage

At thermodynamic equilibrium, the terminal voltage of a lead/acid battery adjusts to an equilibrium voltage $V_0$ that depends mainly on the electrolyte concentration and, thus, on the SOC. A sufficient approximation for the equilibrium voltage depending on the molality $m$ in mol/kg at 25 °C is according to Ref. [4]

$$\frac{V_0(m)}{V} = 1.9228 + 0.147519 \log m + 0.063552(\log m)^2 + 0.073772(\log m)^3 + 0.033612(\log m)^4 \quad (1)$$

where 1 mole electrolyte is consumed by drawing an electrical charge of 1 F from the battery. The average molality of sulfuric acid calculated over the complete battery may then be derived as a function of the drawn charge $Q_e$

$$m(Q_e) = m_{\text{Batt full}} - \frac{Q_e}{FM_{el}} \quad (2)$$

where $m_{\text{Bat full}}$ represents the electrolyte molality of a completely charged battery; it has usually an amount of $m_{\text{Batt full}} = 6.25$ mol/kg [5]. $M_{el}$ stands for the electrolyte mass and depends on the type and the nominal capacity of the battery.

In the case of sealed batteries, it is difficult to measure the electrolyte mass. Therefore, the electrolyte mass and molality are derived for full SOC by parameter fitting to measured values. Fig. 4 illustrates this technique for a Sonnenschein dry-fit traction block, Model 6V-160.

At first, the equilibrium voltage as a function of the molality is linearized in one operating point in order to calculate the electrolyte mass. The molality of the completely charged battery is chosen as the operating point. In this way, the following can be derived

$$V_0(m) \approx V_0|_{m=6.25\,mol/kg} + \Delta m \left.\frac{dV_0}{dm}\right|_{m=6.25\,mol/kg}$$

where $\Delta m = m - 6.25$ mol/kg, and

$$\frac{V_0(m)}{V} \approx 1.917 + 0.0329 \frac{m}{\text{mol/kg}}$$

The terminal voltage gradient of a single battery cell can be deduced from Fig. 4

$$\frac{\Delta V_0}{\Delta Q_e} \approx \frac{1}{750} \frac{V}{\text{Ah}}$$

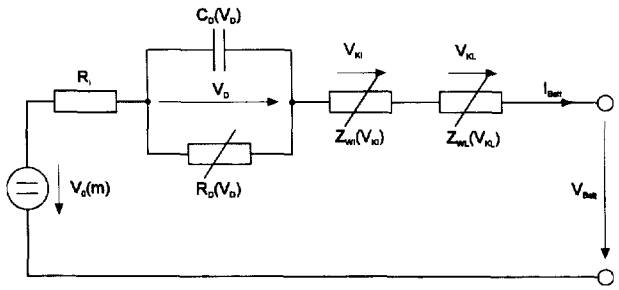


Fig. 3. Simplified complete equivalent circuit of a lead/acid battery based on Randles' theory.

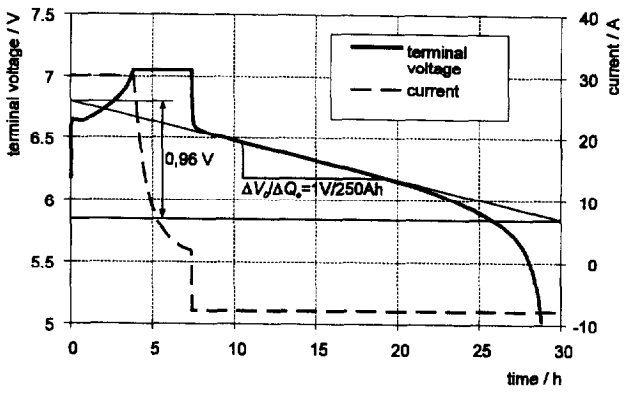


Fig. 4. Adapting the dependence of equilibrium voltage on state-of-charge for a Sonnenschein dry-fit traction block 6V-160.

This leads to an electrolyte mass per cell of the Sonnenschein dry-fit traction block 6V-160 as approximately

$$M_{el} \approx \frac{\Delta Q_e}{F \Delta V_0} \frac{dV_0}{dm}\bigg|_{m=6.25\,mol/kg} = 0.92\,kg$$

Eqs. (1) and (2) describe the dependence of the equilibrium voltage $V_0$ on the drawn charge $Q_e$. With this connection, the block diagram of the equilibrium-voltage model in Matlab–Simulink (Fig. 5) can be derived.

### 3.2. Modelling the electrically conductive media

The finite conductivity of all electrically conductive media within the battery (especially within the electrolyte) causes a voltage drop. This effect is often termed as 'polarization'. Since the electrolyte conductivity can be considered as constant for concentrations higher than 2 mol/kg [4], a constant equivalent resistance $R_i$ is used for modelling the battery resistance. According to our measurements of the Sonnenschein dry-fit traction block 6V-160, this equivalent resistance $R_i$ is 0.65 mΩ per cell.

### 3.3. Modelling the double-layer capacitance

The overvoltage at the electrolytic double-layer depends on the charge stored in the double layer. This can be described by a differential double-layer capacitance which is a function of the voltage at the double layer and is given by Ref. [6]

$$\tilde{C}_D(V_D) = \frac{dQ_D}{dV_D} = A_E \sqrt{\frac{2c_i|_{x=0} \epsilon z^2 F^2}{RT}} \cosh\left(\frac{zFV_D}{2RT}\right) \tag{3}$$

After renaming the constants in Eq. (3), Eq. (4) is derived

$$\tilde{C}_D(V_D) = c_{D1} \cosh(c_{D2} V_D) \tag{4}$$

The constants $c_{D1}$ and $c_{D2}$ are experimentally obtained from impedance spectra as a function of the overvoltage $\overline{V}_D$ (see Section 3.4). Fig. 6 shows the fit result that is based on a least-square algorithm.

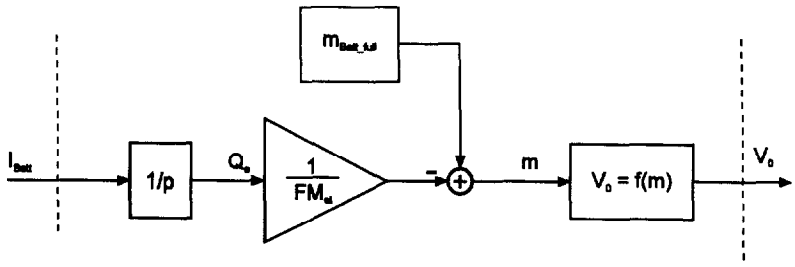


Fig. 5. Equilibrium-voltage block diagram of the lead/acid battery in Matlab–Simulink.

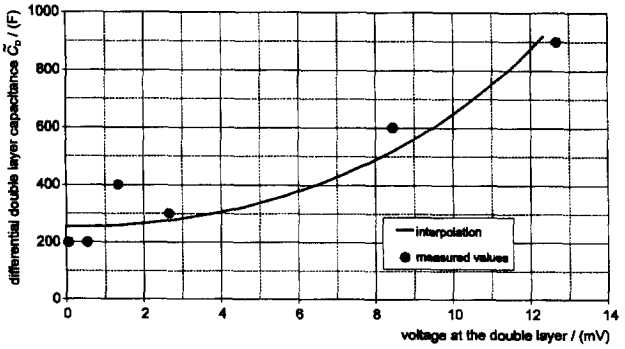


Fig. 6. Fitting the parameters $c_{D1}$ and $c_{D2}$ of the differential double-layer capacitance to the measured impedance data of a Sonnenschein dry-fit traction block 6V-160 ($c_{D1} = 252.7$ F, $1/c_{D2} = 6.28$ mV).

Integrating the differential double-layer capacitance along the overvoltage leads to the charge $Q_D$ stored in the double-layer

$$Q_D = \int_0^{V_D} \tilde{C}_D(V)\mathrm{d}V = \frac{c_{D1}}{c_{D2}} \sinh(c_{D2}V_D) \tag{5}$$

The overvoltage at the double layer results from the inverse function of Eq. (5)

$$V_D = \frac{1}{c_{D2}} \operatorname{arsinh}\left(\frac{c_{D2}}{c_{D1}} Q_D\right) \tag{6}$$

### 3.4. Modelling the charge-transfer resistance

The reaction equilibrium can be altered in the direction of either the charge or the discharge reaction by applying an electric field to the interface. The resulting Faraday current density is described by the Butler–Volmer equation [1,7,8] as a function of the charge-transfer overvoltage $\eta_D$ at the interface

$$i_F = -i_0\left[\exp\left(-\tfrac{nF}{RT}\alpha\eta_D\right) - \exp\left(\tfrac{nF}{RT}(1-\alpha)\eta_D\right)\right] \tag{7}$$

All constants of Eq. (7) are renamed

$$I_F = -\frac{c_{F1}}{2}\left[\exp(-2c_{F2}\alpha V_D) - \exp(2c_{F2}(1-\alpha)V_D)\right] \tag{8}$$

The differential charge-transfer resistance $\tilde{R}_D$ is measured by impedance spectroscopy for some superimposed direct currents $\bar{I}_F$ which cause constant overvoltages $\bar{V}_D$ at the interface.

First, the inverse function of Eq. (8) must be derived for the calculation of $c_{F1}$ and $c_{F2}$. In order to inverse Eq. (8), parameter $\alpha$ has to be adjusted to 0.5. This causes an error that remains small if either charging or discharging is considered

$$I_F = c_{F1} \sinh(c_{F2}V_D) \tag{9a}$$

$$V_D = \frac{1}{c_{F2}} \operatorname{arsinh}\left(\frac{I_F}{c_{F1}}\right) \tag{9b}$$

$$\tilde{R}_D = \frac{\partial\bar{V}_D}{\partial\bar{I}_F} = \frac{\tilde{V}_D}{\tilde{I}_F}\bigg|_{\bar{I}_F} = \frac{1}{c_{F2}} \frac{1}{\sqrt{c_{F1}^2 + \bar{I}_F^2}} \tag{10}$$

Second, the constants $c_{F1}$ and $c_{F2}$ are derived by fitting Eq. (10) to the measured values. The integral performance of the phase transfer can be characterized with help of the Eq. (9). The least-square fit of the parameters is illustrated in Fig. 7 for a Sonnenschein dry-fit traction block 6V-160.

The block diagram of the transfer resistance and the double-layer capacitance in Matlab–Simulink is given in Fig. 8.

### 3.5. Modelling the concentration overvoltage

The dependence of the concentration overvoltage on current and frequency is highly non-linear. The modelling of the concentration overvoltage involves five steps:

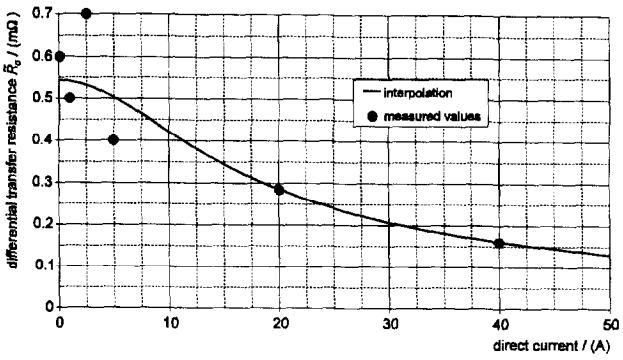


Fig. 7. Parameter fit $c_{F1}$ and $c_{F2}$ of the differential transfer-resistance to themeasured impedance data of a Sonnenschein dryfit traction block 6V-160 ($c_{F1} = 12.4$ A, $1/c_{F2} = 6.70$ mV).

1. linearizing the concentration overvoltage and its small-signal characteristics;
2. measuring the parameters of the small-signal model by impedance spectroscopy for several superimposed direct currents;
3. determining the small-signal parameters as a function of the direct current in each operating point;
4. deriving the large-signal model from integrating the small-signal characteristics along the current or the voltage [9], and
5. transforming the large-signal model back from the frequency into the time domain.

Such non-linear models require numerical integration techniques for solution. But today, this bears no restrictions if modern simulation programs such as Matlab–Simulink are used for calculation.

*3.5.1. Warburg impedance*

During discharging, the sulfuric acid is consumed and a diffusion process starts [8]. In the case of simple diffusion, Warburg gives differential resistances under three different boundary conditions:

(i) The electrolyte has the finite extension $l$ and is limited by a reservoir of constant concentration (ideal reservoir)

$$\underline{\tilde{Z}}_{WI} = \frac{RT}{cz^2F^2A_e}\frac{1}{\sqrt{pD}}\tanh\left(l\sqrt{\frac{p}{D}}\right) \tag{11}$$

where $p = j\omega$.

(ii) The electrolyte has the finite extension $l$ and is limited by a non-permeable wall (no transport of any substance through the wall)

$$\underline{\tilde{Z}}_{WL} = \frac{RT}{cz^2F^2A_e}\frac{1}{\sqrt{pD}}\coth\left(l\sqrt{\frac{p}{D}}\right) \tag{12}$$

(iii) In the limiting case of infinitely extended electrolyte ($l \to \infty$), the two Warburg impedances are equal

$$\underline{\tilde{Z}}_{WI}\big|_{l\to\infty} = \underline{\tilde{Z}}_{WL}\big|_{l\to\infty} = \underline{\tilde{Z}}_{W\infty} = \frac{RT}{cz^2F^2A_e}\frac{1}{\sqrt{pD}} \tag{13}$$

The three different types of the Warburg impedances are illustrated in Fig. 9.

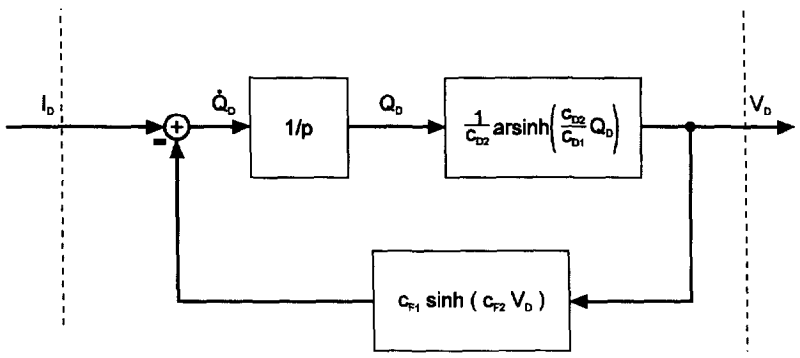


Fig. 8. Block diagram of the transfer-resistance and the double-layer in Matlab–Simulink.

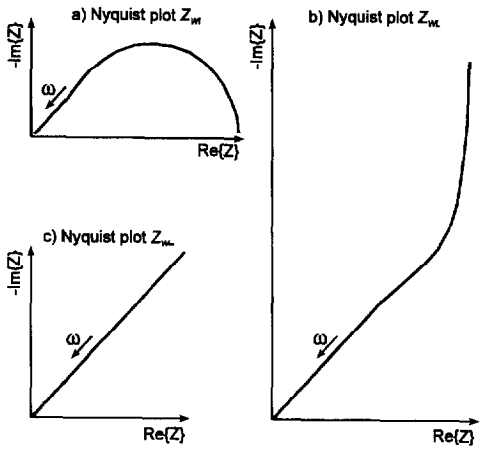


Fig. 9. Nyquist plots of different Warburg impedances: (a) limited diffusion-layer and ideal reservoir at the boundary; (b) limited diffusion-layer and a non-permeable wall at the boundary, and (c) unlimited diffusion layer.

### 3.5.2. *Discussion of boundary conditions*

Since the electrolyte within the battery is spatially limited, the electrolyte cannot diffuse through this boundary from outside towards inside. A dynamic performance is expected here as it is described by the Warburg impedance $\underline{\tilde{Z}}_{WL}$ (see Fig. 9(b)). The results of experimental measurements rather show, however, a resemblance to the Warburg impedance $\underline{\tilde{Z}}_{WI}$ (see Fig. 9(a)). Only at very low frequencies ($f \leq 20$ μHz, $I_{DC} = 0.1$ A) can a performance according to $\underline{\tilde{Z}}_{WL}$ be measured.

This effect can be explained by assuming a different composition of the several diffusion zones [10]. A sectional view through a lead/acid battery is given in Fig. 10. The area filled with electrolyte can be zoned twice:

(A) The channels inside the porous electrode material can be modelled by cylinders vertical to the electrode surface. In this case, the geometry of diffusion inside the porous electrode material is described by the effective diffusion length $l^*$ and the effective area $A^*$. For the boundary between the plates and the electrolyte, a condition according to (i) in Section 3.5.1 and thus a Warburg impedance $\underline{\tilde{Z}}_{WI}$, is assumed.

(B) Diffusion exists between the plates in the gelled electrolyte and in the separator. Even here, it can be assumed that the diffusion coefficient for the gelled electrolyte is smaller than that for free electrolyte. Given a diffusion process vertical to the electrode surfaces, the diffusion length is of the order of 1 mm. The assumption in (A) that diffusion has only one spacial component is here no longer valid for the area between the plates. The inhomogeneous current distribution within the plates [11] leads to an inhomogeneous acid stratification in the space between the plates. It is compensated by diffusion in parallel with the surfaces of the plates. In contrast to diffusion vertical to the surfaces of the plates, the diffusion area is much smaller and the diffusion length now much larger. Here, a boundary conditions according to (ii) in Section 3.5.1 can be assumed and the Warburg impedance $\underline{\tilde{Z}}_{WL}$ is applied.

For steady-state operation, Ref. [10] assumes two different diffusion layers in order to characterize the battery capacity as a function of the discharge current. A significant improvement of this function compared with that of Peukert is reached in that way. In this paper, two Warburg impedances are also applied for the characterization of the dynamic performance that describe separately the different diffusion mechanisms inside and outside the plates. As can be seen in Fig. 11, the

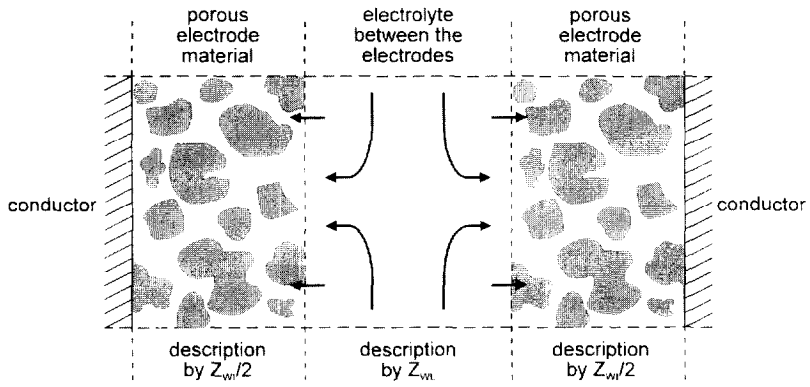


Fig. 10. Sectional view through a lead/acid cell. The direction of diffusion in the electrolyte is marked with arrows for discharging.

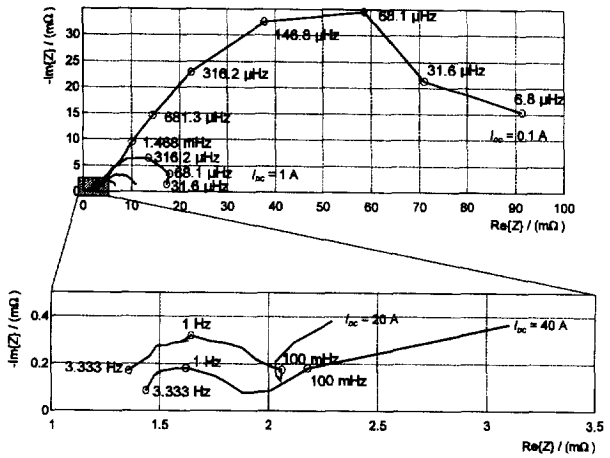


Fig. 11. Nyquist plots of a Sonnenschein dry-fit traction block 6V-160 measured by impedance spectroscopy at different direct currents. The magnification in the lower part of the figure contains only the two invisible curves of the upper part. All other curves are suppressed in the magnification to give a clear illustration.

performance according to $\underline{\tilde{Z}}_{WI}$ or $\underline{\tilde{Z}}_{WL}$ can be very well distinguished only for small superimposed direct currents. $\underline{\tilde{Z}}_{WL}$ is negligible for small direct currents because of its relevance only for very small frequencies. But the performance of the battery is strongly influenced by $\underline{\tilde{Z}}_{WL}$ in the case of increasing direct currents. Therefore $\underline{\tilde{Z}}_{WI}$ and $\underline{\tilde{Z}}_{WL}$ are included in the battery model.

### 3.5.3. *Interpretation of the differential concentration model as an equivalent electric circuit*

Only the Warburg impedance $\underline{\tilde{Z}}_{WI}$ is considered in the following. The calculation of $\underline{\tilde{Z}}_{WL}$ runs corresponding to this (complete derivation in Ref. [12]). The application of transport modelling in simulation programs requires the transformation of $\underline{\tilde{Z}}_{W}$ back into the time domain. According to Ref. [13], the impulse response of the Warburg impedance $\underline{\tilde{Z}}_{WI}$ derives as (11)

$$\frac{k_{I2}}{\sqrt{p}}\tanh\left(\frac{k_{I1}}{k_{I2}}\sqrt{p}\right)\bullet\!-\!\circ\,\frac{2k_{I2}^2}{k_{I1}}\sum_{n=1}^{\infty}\exp\left(\frac{(2n-1)^2\pi^2k_{I2}^2}{4k_{I1}^2}t\right) \tag{14}$$

$$k_{I2}=\frac{RT}{cz^2F^2A_e\sqrt{D}}$$

with

$$k_{I1}=\frac{l}{\sqrt{D}}k_{I2}=\frac{RTl}{cz^2F^2A_eD}$$

The constants $k_{I1}$ and $k_{I2}$ depend only on the d.c. component of the current flowing through the Warburg impedance. The weak dependence on the average electrolyte concentration, in other words, on the battery state-of-charge is neglected. The comparison of the impulse response of the Warburg impedance with the impedance of an RC-circuit

$$\frac{1/C}{p+1/RC}\bullet\!-\!\circ\,\frac{1}{C}\exp(-t/RC)$$

shows that the Warburg impedance can be interpreted as a serial connection of an infinite number of *RC* circuits. The impulse response $h(t)$ of this serial connection has the form

$$h_I(t)=\sum_{n=1}^{\infty}\frac{1}{C_{KIn}}\exp\left(-\frac{t}{R_{KIn}C_{KIn}}\right)$$

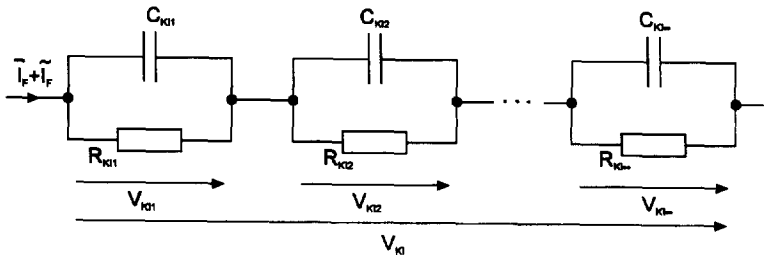


Fig. 12. Equivalent electric circuit of the serial *RC*-connection used for the approximation of the Warburg impedance $Z_{WI}$.

$R_{KIn}$ and $C_{KIn}$ are found by comparison of the coefficients in Eq. (14)

$$C_{KIn} = \frac{k_{I1}}{2k_{I2}^2} = \frac{cz^2F^2A_e l}{2RT} \tag{15a}$$

$$R_{KIn} = w_{In}k_{I1} = w_{In}\frac{RTl}{cz^2F^2A_e D} \tag{15b}$$

$$w_{In} = \frac{8}{(2n-1)^2\pi^2} \tag{15c}$$

$$\sum_{n=1}^{\infty} w_{In} = 1 \tag{15d}$$

Fig. 12 shows the equivalent electric circuit of the serial *RC* connection that is used for the approximation of the Warburg impendence $Z_{WI}$.

### 3.5.4. Parameter determination of the differential concentration model

After measuring several impedance spectra for different superimposed direct currents, the parameters $k_{I1}$ and $k_{I2}$ of the Warburg impedance $\tilde{Z}_{WI}$ are determined now as a function of the operating point. The parameter $k_{I1}$ affects the intersection of the impedance curve with the real axis at low frequencies and is therefore called $R_{K1}$ (cf., Fig. 2). The Parameter $k_{I2}$ influences the frequency scaling and thus is adjusted in a second step. In Fig. 13, the adaptation of the battery model to a measured Nyquist plot is given for a superimposed direct current of $I_{DC} = 2.5$ A. The upper half of the figure shows the adaptation without taking $Z_{WL}$ into account. For very low frequencies, the deviation between the model and measurement becomes significant. The lower half of the figure shows the results of adaptation if $Z_{WL}$ is taken into account. Here, a very good correspondence between model and measurement can be seen particularly at low frequencies.

The parameters $k_{I1}$, $k_{I2}$, $k_{L1}$ and $k_{L2}$ are given in Table 2 for several direct currents.

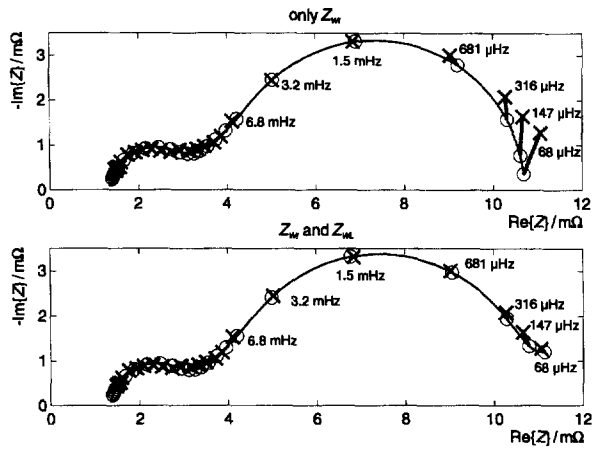


Fig. 13. Parameter adaptation of the battery model to a measured Nyquist plot for $I_{DC} = 2.5$ A. Top curve: without taking the impedance $Z_{WL}$ into account; bottom curve: taking the impedance $Z_{WL}$ into account. Crosses: measured values at different frequencies. Circles: corresponding model performance. Thin lines: performance of the modelling; thick lines: deviation between modelling and measurement.

Table 2
Measured parameters of the concentration model for a Sonnenschein dry-fit traction block 6V-160

| $I_{DC}$ (A) | $k_{I1}$ (Ω) | $k_{I2}$ (Ω/s$^{1/2}$) | $k_{L1}$ (Ω) | $k_{L2}$ (Ω/s$^{1/2}$) |
|---|---|---|---|---|
| 0.1 | 0.03750 | 0.000575 | 0.25 | 0.0000125 |
| 1 | 0.00775 | 0.000260 | 0.25 | 0.0000090 |
| 2.5 | 0.00380 | 0.000210 | 0.23 | 0.0000125 |
| 5 | 0.00235 | 0.000145 | 0.19 | 0.0000115 |
| 20 | 0.00040 | 0.000064 | 0.07 | 0.0000125 |
| 40 | 0.00020 | 0.000055 | 0.03 | 0.0000125 |

*3.5.5. Transition to integral performance of the concentration overvoltage*

For the transition of the concentration overvoltage from differential to integral performance, a connection must be found between the parameters $k_{I1}$ and $k_{I2}$ and the superimposed d.c. component of the current. At first, the parameter $k_{I1}$ is examined and is determined only by the steady-state performance of the concentration element.

A constant current flowing for a very long time is equivalent to a stationary concentration gradient (time-invariant) within the electrolyte. The three-dimensional structure of the gradient determines the stationary concentration overvoltage $\bar{V}_K$. Its dependence on the current $\bar{I}_K$ is assumed to be the general solution of an ordinary differential equation of second order (this assumption is verified by experiments explained later)

$$\bar{I}_{KI} = A\exp\left(B\bar{V}_{KI}\right) - C\exp D\bar{V}_{KI})$$

with constants $A$, $B$, $C$ and $D$. Setting the boundary condition $\bar{V}_{KI}|_{\bar{I}_{KI}} = 0$ requires $A = C$. Renaming the coefficients leads to

$$\bar{I}_{KI} = c_{KI1}\left[\exp\left(c_{KI2}\bar{V}_{KI}\alpha\right) - \exp\left(-c_{KI2}\bar{V}_{KI}(1-\alpha)\right)\right] \tag{16}$$

Our experiments show that the simplification $\alpha = 0.5$ causes large errors and thus is not permitted (contrary to Section 3.4). The differential concentration resistance $\tilde{R}_{KI}$ was determined for several operating points by impedance measurements as a function of the superimposed direct current $\bar{I}_{KI}$ through the concentration element. A simple parameter identification (as used in Section 3.4) requires the differentiated inverse function of Eq. (16). Since it is not possible to determine the inverse function analytically, an iteration technique is used here. First, the differential quotient of Eq. (16) is built for this purpose

$$\frac{\mathrm{d}\bar{I}_{KI}\left(\bar{V}_{KI}\right)}{\mathrm{d}\bar{V}_{KI}} = \lim_{h\to 0}\frac{\bar{I}_{KI}\left(\bar{V}_{KI}+h\right) - \bar{I}_{KI}\left(\bar{V}_{KI}\right)}{h} \tag{17}$$

The differential concentration resistance is given with this expression as a function of $\bar{V}_{KI}$

$$\tilde{R}_{KI}\left(\bar{V}_{KI}\right) = \lim_{h\to 0}\frac{h\bar{V}_{KI}}{\bar{I}_{KI}\left(\bar{V}_{KI}+h\right) - \bar{I}_{KI}\left(\bar{V}_{KI}\right)} \tag{18}$$

The $m$ measured values of the differential concentration resistance are known to be a function of the direct current $\bar{I}_{KI}$ and not of the voltage $\bar{V}_{KI}$

$$\tilde{R}_{KI\nu}\left(\bar{I}_{KI\nu}\right) \text{ for } \nu = (1\cdots m)$$

Since the voltage at the concentration element is not directly measurable, $\tilde{R}_{KI}$ cannot be measured as a function of $\bar{V}_{KI}$. The two-staged iteration procedure which is used for the calculation of the parameters $c_{KI1}$, $c_{KI2}$ and $\alpha_{KI}$ is as follows:

(i) step 1: suitable values are estimated for the parameters $c_{KI1}$, $c_{KI2}$ and $\alpha_{KI}$;

(ii) step 2: calculation of $m$ values of the voltages $V_{KI\nu}$ with the help of a Newton method leads to

$$\bar{I}_{KI\nu} = c_{KI1}\left[\exp\left(c_{KI2}\bar{V}_{KI\nu}\alpha_{KI}\right) - \exp\left(-c_{KI2}\bar{V}_{KI\nu}(1-\alpha_{KI})\right)\right] \text{ for } \nu = (1\cdots m)$$

(iii) step 3: the parameters $c_{KI1}$, $c_{KI2}$ and $\alpha_{KI}$ are found with the help of a Newton method by minimizing the square error $F$ between the measured and calculated differential concentration resistance

$$F = \min\left(\lim_{h\to 0}\sum_{\nu=1}^{m}\left[\tilde{R}_{KI\nu} - \frac{h\bar{V}_{KI\nu}}{c_{KI1}\left[\exp\left(c_{KI2}\left(\bar{V}_{KI}+h\right)\alpha_{KI}\right) - \exp\left(-c_{KI2}\left(\bar{V}_{KI}+h\right)(1-\alpha_{KI})\right) - \exp\left(c_{KI2}\bar{V}_{KI}\alpha_{KI}\right) + \exp\left(-c_{KI2}\bar{V}_{KI}(1-\alpha_{KI})\right)\right]}\right]^2\right)$$

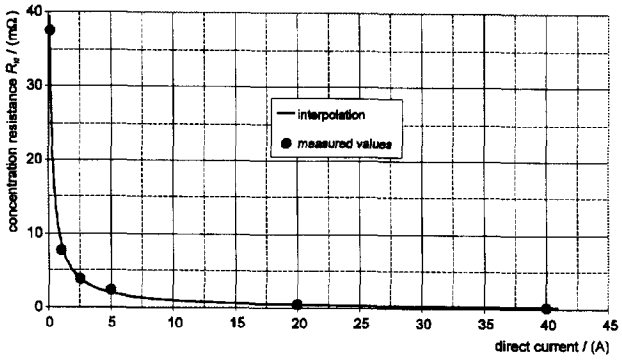


Fig. 14. Fitting the parameters $c_{KI1}$ and $c_{KI2}$ of the concentration resistance $R_{KI}$ to the measured resistance data of a traction battery-type Sonnenschein dryfit traction block 6V-160 ($c_{KI1} = 0.1245$ A, $1/c_{KI2} = 5.52$ mV, $\alpha = 0.628$).

(iv) step 4: step 2 of this procedure is repeated until the parameters $c_{KI1}$, $c_{KI2}$ and $\alpha_{KI}$ are sufficiently stable.

Fig. 14 compares the interpolation result with the measured values.

The concentration resistance $\tilde{R}_{KIn}(I_{Kn})$ of a partial element in the concentration model is calculated by multiplying the complete concentration resistance $R_{KI}(\bar{I}_K)$ with the factor $w_{In}$ according to Eq. (15). With this, the current $I_{KIn}$ through every partial concentration element is

$$I_{KIn} = c_{KI1}\left[\exp\left(\frac{c_{KI2}V_{KI}\alpha}{w_{In}}\right) - \exp\left(-\frac{c_{KI2}V_{KI}(1-\alpha)}{w_{In}}\right)\right] \tag{19}$$

The differential concentration capacitances read as follows

$$\tilde{C}_{KIn}(\tilde{I}_{KIn}) = \frac{\mathrm{d}\bar{Q}_{KIn}}{\mathrm{d}\bar{V}_{KIn}} = \left.\frac{\tilde{Q}_{KIn}}{\tilde{V}_{KIn}}\right|_{\tilde{I}_{KIn}} = \frac{k_{I1}(\bar{I}_K)}{2k_{I2}^2(\bar{I}_K)} \tag{20}$$

$\tilde{C}_{KIn}$ can be determined by the differentiation of the stationary quantities or by the division of the differential quantities, thus illustrating the connection between differential and integral performance. The constants $k_{I1}$ and $k_{I2}$ are measured as a function of the direct current $\bar{I}_K$. The principle of charge conservation is not broken by the concentration capacitance $\tilde{C}_{Kn}$ depending on $\bar{I}_K$ because all d.c. components flow through the concentration resistance. Only if the concentration capacitance was a function of the a.c. component $\tilde{I}_{Kn}$, the law would be broken.

A calculation is quite comfortable if a capacitance depends only on the voltage. Therefore, the dependence on the direct current $\tilde{I}_{KIn} = \bar{I}_K$ which flows through the concentration element is converted into a dependence on the voltage at the concentration resistance $\bar{V}_{KIn}$. With

$$\bar{V}_{KIn} = w_{In}\bar{V}_{KI}$$

and Eq. (20) it leads to

$$\tilde{C}_{KIn}(\bar{V}_{KIn}) = \frac{k_{I1}(\bar{V}_{KI})}{2k_{I2}^2(\bar{V}_{KI})} = \frac{k_{I1}\left(\frac{\bar{V}_{KIn}}{w_{In}}\right)}{2k_{I2}^2\left(\frac{\bar{V}_{KIn}}{w_{In}}\right)} \tag{21}$$

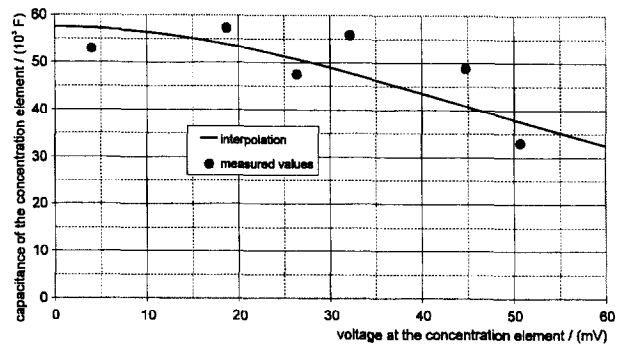


Fig. 15. Fitting parameters $c_{KI3}$ and $c_{KI4}$ of the concentration capacitance $C_{KI}$ to the performance of a Sonnenschein dry-fit traction block 6V-160 ($c_{KI3} = 57500$ F, $1/c_{KI4} = 51.3$ mV).

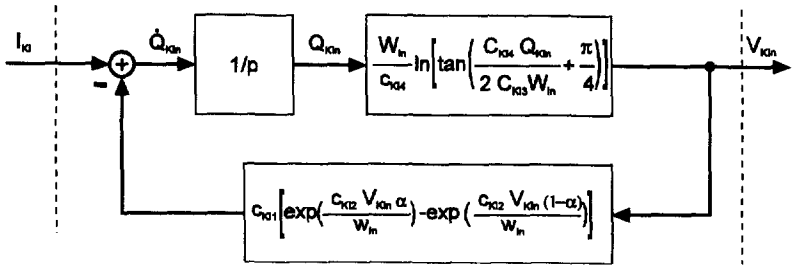


Fig. 16. Block diagram of a single concentration element $R_{KIn}$.

Eq. (21) is valid if only a direct current flows through the concentration element. If time-variable currents are allowed, it must read

$$\tilde{C}_{KIn}(V_{KIn}) = \frac{k_{I1}\left(\frac{V_{KIn}}{w_{In}}\right)}{2k_{I2}^2\left(\frac{V_{KIn}}{w_{In}}\right)}$$

The following expression turned out to be a good description for the dependence on the voltage at differential concentration capacitances

$$\tilde{C}_{KIn}(V_{KIn}) = \frac{c_{KI3}}{\cosh\left(\frac{c_{KI4}V_{KIn}}{w_{In}}\right)} \tag{22}$$

An example for fitting $c_{KI3}$ and $c_{KI4}$ to measured values can be seen in Fig. 15.

The charge of every single concentration capacitor is calculated by integration as

$$Q_{KIn} = \int_0^{U_{KIn}} c_{KI3}\left[\cosh\left(\frac{c_{KI4}V}{w_{In}}\right)\right]^{-1} \mathrm{d}V = \frac{2c_{KI3}w_{In}}{c_{KI4}}\left[\arctan\left[\exp\left(\frac{c_{KI4}V_{KIn}}{w_{In}}\right)\right] - \frac{\pi}{4}\right] \tag{23}$$

With that, an expression for the voltage at the concentration element is found as a function of the stored charge

$$V_{KIn} = \frac{w_{In}}{c_{KI4}}\ln\left[\tan\left(\frac{c_{KI4}Q_{KIn}}{2c_{KI3}w_{In}} + \frac{\pi}{4}\right)\right] \tag{24}$$

### 3.5.6. Modelling the concentration overvoltage in Matlab–Simulink

Modelling the concentration overvoltages contains the description of the integral performance of $Z_{WI}$ as well as of $Z_{WL}$. Since both modellings are set up in Matlab–Simulink quite similarly, only the modelling of $Z_{WI}$ is discussed in this Section.

Eqs. (15) and (24) describe the diffusion performance of the lead/acid battery according to $Z_{WI}$. Now, the process of modelling takes place in the state space. At first, the non-linear differential equations that describe the diffusion performance of a single concentration element are given as a block diagram (Fig. 16).

```
function [sys, x0] = warburg(t,x,u,flag,c)
% Warburg-Impedanz

wi = 8./([1:c(6)]'.*2-1).^2./pi^2;

if flag==0
   sys = [c(6);0;1;1;0;0];
   x0  = wi.*0;

elseif flag==1
   U = wi./c(5).*asinh(c(5).*x./c(4)./wi);
   sys = - c(1)*(exp(c(3)*c(2)*U./wi)-exp(-(1-c(3))*c(2)*U./wi)) +u(1)

elseif flag==3
   sys = sum( wi./c(5).*asinh(c(5).*x./c(4)./wi) );
else
   sys = [];
end
```

Fig. 17. Concentration model according to Warburg realized in Matlab–Simulink for a finite diffusion length which is limited by an ideal electrolyte reservoir.

The charge $Q_{KIn}$ is chosen as the state variable, the current $I_K$ is input and the concentration overvoltage $V_{KIn}$ is output variable. The derivative of the state variable in time as well as the output variable must be set up as a linear combination of the input and the state variable

$$\dot{Q}_{KIn} = -c_{KI1}\left[\exp\left[\frac{c_{KI2}}{c_{KI4}}\alpha_{KI}\,\mathrm{arsinh}\left(\frac{c_{KI4}Q_{KIn}}{c_{KI3}w_{In}}\right)\right] - \exp\left[-\frac{c_{KI2}}{c_{KI4}}(1-\alpha_{KI})\,\mathrm{arsinh}\left(\frac{c_{KI4}Q_{KIn}}{c_{KI3}w_{In}}\right)\right]\right] + I_k \tag{25}$$

$$V_{KIn} = \frac{w_{In}}{c_{KI4}}\ln\left[\tan\left(\frac{c_{KI4}Q_{KIn}}{2c_{KI3}w_{In}} + \frac{\pi}{4}\right)\right]$$

The complete concentration overvoltage $V_{KI}$ results from the addition of the overvoltages $V_{KIn}$ at all concentration elements. This connection is taken into account by setting up the state variable as a vector $\vec{Q}_{KI}$, the order of which is equal to the number of partial concentration elements. Corresponding to this, a vector $\vec{V}_{KI}$ is used which contains the overvoltages at every concentration element. Vector $\vec{w}_I$ sets the weighting factors. The input $I_K$ remains a scalar because the same current $I_K$ flows through all concentration elements.

With the function

$$\mathrm{sum}(\vec{V}) \overset{\mathrm{def}}{=} \sum_{i=1}^{n} v_i \quad \text{with } \vec{V} = (v_1, v_2, \cdots, v_n)$$

the state equations are written as

$$\dot{\vec{Q}}_{KI} = -c_{KI1}\left[\exp\left[\frac{c_{KI2}}{c_{KI4}}\alpha_{KI}\,\mathrm{arsinh}\left(\frac{c_{KI4}\vec{Q}_{KIn}}{c_{KI3}\vec{w}_{In}}\right)\right] - \exp\left[-\frac{c_{KI2}}{c_{KI4}}(1-\alpha_{KI})\,\mathrm{arsinh}\left(\frac{c_{KI4}\vec{Q}_{KIn}}{c_{KI3}\vec{w}_{In}}\right)\right]\right] + I_K \tag{26}$$

$$V_{KI} = \mathrm{sum}\left[\frac{\vec{w}_I}{c_{KI4}}\ln\left[\tan\left(\frac{c_{KI4}\vec{Q}_{KI}}{2c_{KI3}\vec{w}_I} + \frac{\pi}{4}\right)\right]\right]$$

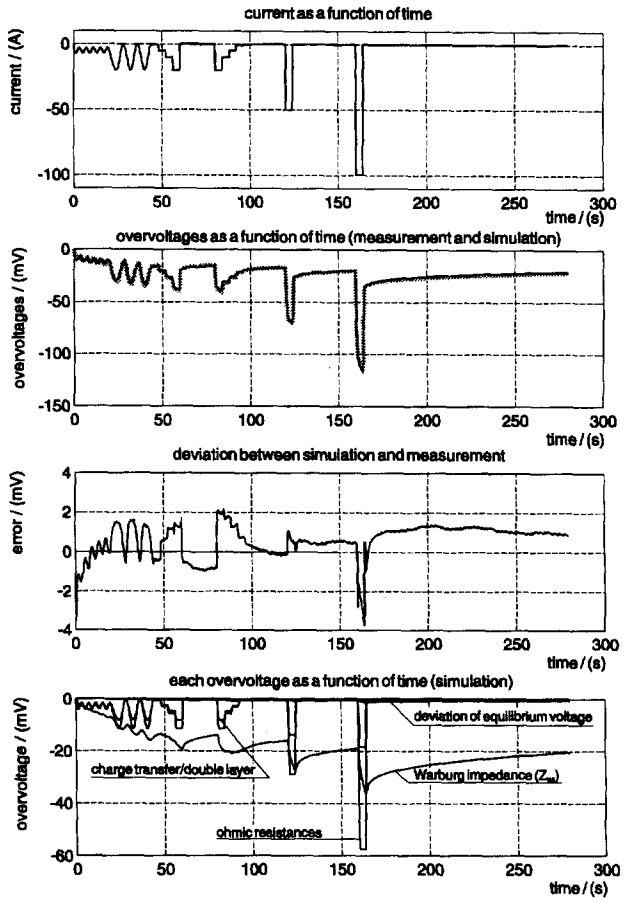


Fig. 18. Diagram 1: current; diagram 2: overvoltage per cell (grey: measurement; black: simulation); diagram 3: deviation between simulation and measurement, and diagram 4: division of the overvoltages according to their physical causes.

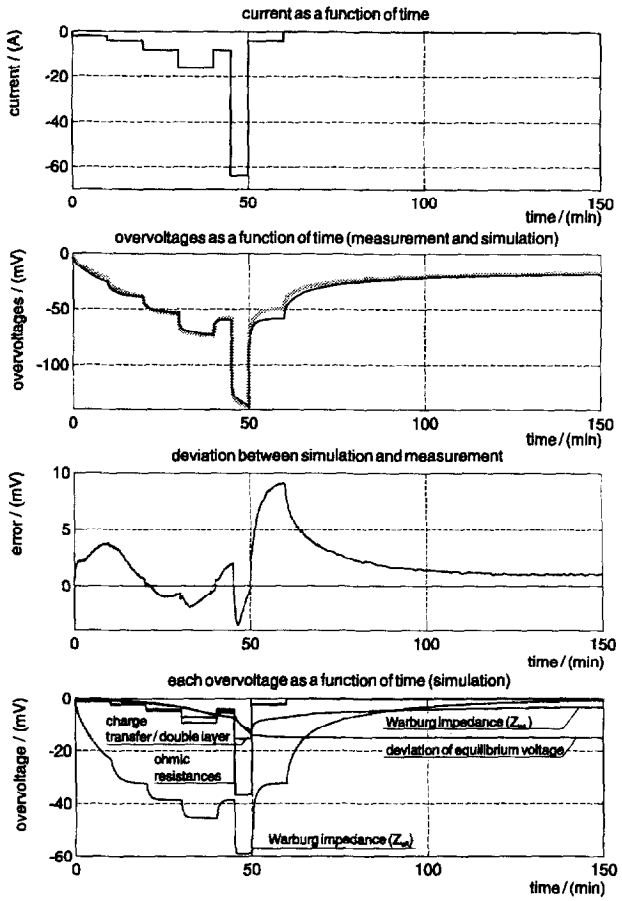


Fig. 19. Diagram 1: current; diagram 2: overvoltage per cell (grey: measurement; black: simulation); diagram 3: deviation between simulation and measurement, and diagram 4: division of the overvoltages according to their physical causes.

Please note that the argument of the inverse hyperbolic sine is not a vector division but a division element by element. Vectors with infinite dimensions cannot be technically realized. Therefore, the sum is finished with the element $z$.

This causes an error in thermodynamic equilibrium state of

$$V_{KI_{\text{Error}}} = -\left(1 - \sum_{n=1}^{z} w_{In}\right) V_{KI} \tag{27}$$

If the number $z$ of partial concentration elements is chosen sufficiently high, this error is negligible. The conversion of the state equations into an 'S-function' in Matlab–Simulink is shown in Fig. 17.

## 4. Verification of the battery model and discussion of the results

It is necessary to verify the battery model in order to evaluate its quality. This verification has to be based on new measurements which are not previously used to determine any model parameter. Usually, the validity of any complex model cannot be proven completely. Therefore, a model verification should examine precisely those states of operation that dominate in the application of the model.

Three different experiments were conducted in order to verify our model of the lead/acid battery. The experiments differ in frequency and amplitude of the current, and they approximate the real battery operation in an electric vehicle. The Figs. 18–20 illustrate the experiments. In all experiments, the battery current is given as a function of time plotted in the first diagram of each figure. Below, the second diagram shows the battery voltage response per cell (measured: grey, as well as simulation result: black). The deviation between measured and simulated voltage, as plotted in the third diagram, allows evaluation of the quality of the battery model. The last diagram shows the division of all overvoltages according to their physical causes. It is used to judge the relevance of every single overvoltage mechanism and thus the relevance of each part of the battery model.

The experiment with a duration of 300 s (Fig. 18) examines the model at higher frequencies. Here, the model performance under fast load changes is characterized. The deviation between measured and simulated value stretches over a

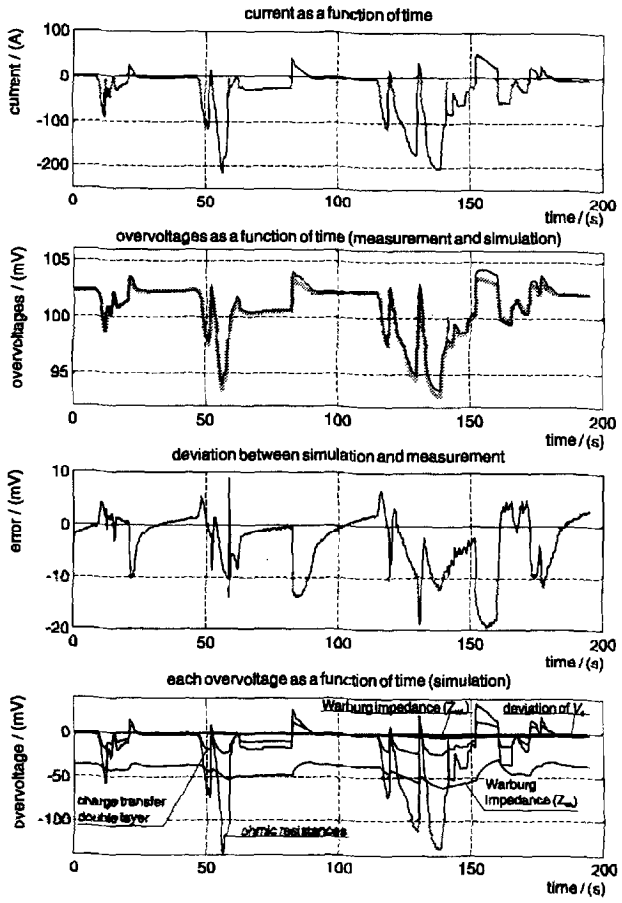


Fig. 20. Diagram 1: current; diagram 2: overvoltage per cell (grey: measurement; black: simulation); diagram 3: deviation between simulation and measurement, and diagram 4: division of the overvoltages according to their physical causes.

range of $\pm 2$ mV except for one interval. This performance is equivalent to a model error of only $\pm 0.1\%$ related to the battery terminal voltage.

During the experiment shown in Fig. 19, the battery is discharged by $\sim 10\%$. It serves as a verification for the long-time stability of the model. Here, the deviation between measured and simulated cell voltages is smaller than $\pm 4$ mV which corresponds to a model error of $\pm 0.2\%$. Only after switching off high currents (see Fig. 19 between $t = 50$ min and $t = 60$ min) the error doubles. This effect is probably caused by neglecting the migration mechanism (see Section 3.5).

The experiment referred to in Fig. 20 is the most realistic test of the battery model. Here, the terminal voltage and the battery current were measured on a dynamometer during one phase of an ECE cycle in a CitySTROMer type A3. The vehicle was equipped with a Sonnenschein dry-fit traction block 6V-160. For simulation, the measured current was used as input of the battery model. As a result, the simulated voltage characteristic of 48 serial-connected cells deviates from the measured only about 1 V maximum. The model parameters were not measured at the CitySTROMer battery but at a much older one. Nevertheless, the extraordinarily good results make this battery model very convincing. This demonstrates the stability of the battery model against ageing, state-of-charge and temperature. Moreover, the model performance is satisfactory even during intermittent charging caused by regenerative braking.

## 5. List of symbols

| | |
|---|---|
| $A_e$, $A^*$ | surface (area) of the interface, effective |
| $c$, $c_i$ | concentration |
| $C_D$, $\tilde{C}_D$ | double-layer capacitance, differential |
| $c_{D1}$, $c_{D2}$ | parameter of the electrolytic double-layer model |
| $c_{F1}$, $c_{F2}$ | parameter of the charge-transfer model |
| $c_{KI1}$, $c_{KI2}$, $\alpha_{KI}$ | parameter of the concentration model (infinite electrolyte layer) |
| $C_{KI}$, $C_{KIn}$ | capacitance of the concentration model, single part element |
| $D$ | diffusion constant |

| | |
|---|---|
| $F$ | Faradayic constant |
| $\tilde{G}_D$ | differential charge-transfer admittance |
| $h(t)$ | impulse response |
| $I$, $I_{DC}$, $i$ | electric current, direct current, current density |
| $i_0$ | exchange current density |
| $I_F$, $\bar{I}_F$, $\tilde{I}_F$, $i_F$ | Faraday part of the current, current density |
| $I_{KI}$, $I_{KIn}$ | current through the concentration element |
| $I_P$, $i_P$ | current which polarizes the electrolytic double layer |
| $k_{I1}$, $k_{I2}$ | parameter of the Warburg impedance |
| $l$, $l^*$ | length of the diffusion layer, effective length |
| $m$, $m_{Batt\ full}$ | molality, molality of a completely charged battery |
| $M_{el}$ | mass of the electrolyte |
| $Q$, $Q_D$, $Q_e$ | charge, charge stored in the electrolytic double layer, withdrawn charge |
| $Q_{KIn}$, $\bar{Q}_{KIn}$ | charge of a single concentration element |
| $R$ | gas constant |
| $R_D$, $\tilde{R}_D$ | charge-transfer resistance, differential |
| $R_i$ | equivalent resistance |
| $R_{KI}$, $R_{KIn}$ | concentration resistance, resistance of a single concentration element |
| $T$ | temperature |
| $V_0$ | equilibrium voltage |
| $V_D$ | voltage at the electrolytic double layer |
| $V_{KI}$, $V_{KIn}$ | voltage at the concentration model, voltage at a single concentration element |
| $w_{KIn}$ | weighting factor |
| $Z$ | impedance |
| Re{$Z$}, Im{$Z$} | real part of the impedance, imaginary part of the impedance |
| $\tilde{Z}_{WI}$, $\tilde{Z}_{WL}$ | differential Warburg impedance for infinite and finite diffusion layer |

*Greek letters*

| | |
|---|---|
| $\alpha$ | activity |
| $\eta_D$, $\bar{\eta}_D$, $\tilde{\eta}_D$ | charge-transfer overvoltage: integral part, direct part, differential part |
| $\epsilon$, $\epsilon_0$, $\epsilon_r$ | dielectric constant, of free space, related |
| $\mu$ | charge carrier mobility |
| $\tau_D$ | time constant of charge transfer and electrolytic double layer |

## References


[1] K.J. Vetter, *Elektrochemische Kinetik*, Springer, Berlin, 1961, p. 268.
[2] P. Mauracher and E. Karden, Measurement of the ultra-low frequency impedance of lead/acid batteries, *Int. Conf. Lead–Acid Batteries LABAT '96, 3–6 June, Varna, Bulgaria.*
[3] G. Paasch, K. Micka and P. Gersdorf, *Electrochim. Acta, 38* (1993) 2653–2662.
[4] H. Bode, *Lead–Acid Batteries*, Wiley, New York, 1977.
[5] VARTA Batterie AG (ed.): *Bleiakkumulatoren*, VDI-Verlag, Dusseldorf, 11th edn., 1986.
[6] D.C. Grahame, *Chem. Rev., 41* (1947) 441; 474 (see Eq. (47)).
[7] F. Beck and K.-J. Euler, *Elektrochemische Energiespeicher*, Vol. 1, VDE-Verlag, Berlin, 1984.
[8] J.R. Macdonald, *Impedance Spectroscopy*. Wiley, New York, 1987.
[9] E. Philippow, *Nichtlineare Elektrotechnik*. Akademische Verlagsgesellschaft, Geest and Portig, Leipzig, 1971.
[10] N.F. Compagnone, *J. Power Sources, 35* (1991) 97–111.
[11] J. Meiwes, Untersuchungen zur Stromaufteilung in Akkumulatoren. *Ph.D. Thesis*, Aachen University of Technology, 1986.
[12] P. Mauracher, Modellierung und Verbundoptimierung bei Elektrostraßenfahrzeugen, *Ph.D. Thesis*, Aachen University of Technology, 1997.
[13] M.R. Spiegel, *Laplace Transforms*, Schaum, New York, 1965.